# Localization of *Aplysia* Neurosecretory Peptides to Multiple Populations of Dense Core Vesicles

Thane Kreiner, Wayne Sossin, and Richard H. Scheller

Department of Biological Sciences, Stanford University, Stanford, California 94305

*Abstract.* Many neurons in the mollusc *Aplysia* are identifiable and provide a useful model system for investigating the cellular mechanisms used by the neuroendocrine system to mediate simple behaviors. In this study we determined the subcellular localization of eight *Aplysia* neuropeptides using immunogold labeling techniques, and analyzed the size distribution of dense core and granular vesicles in peptidergic neurons. Recent observations demonstrate that many neurons use multiple chemical messengers. Thus, an understanding of the functional significance of co-transmitters requires an analysis of their relative subcellular distributions. The peptides are expressed in a subset of neurons, or the exocrine atrial gland, and are primarily localized to dense core vesicles. Multiple regions of precursors which are cleaved into several components are co-localized. Each neuron has a distinct size distribution of peptide-containing dense core vesicles ranging in size from 65 to 600 nm. The atrial gland contains very large (up to 2 $\mu$m) peptide-containing granules. Single neurons have multiple populations of granules whose quantal sizes agree with predictions based on physical constraints. Some cells contain very large peptide-containing granules which are found in the cell soma and not in processes. Thus, the genetic determination of neuronal cell type includes not only transmitter choices but also multiple modes of packaging the intercellular messengers.

BIOLOGICALLY active peptides are frequently used as extracellular chemical messengers in the central nervous system (CNS)[1] (19, 25, 29). Neuropeptides have a variety of characteristics that distinguish them from the more classical neurotransmitters. For instance, the actions of peptides are less often constrained to the synapse. In addition, peptides are synthesized as parts of larger precursors in the cell soma, whereas small molecule transmitters are most often synthesized in the nerve terminal (3, 9, 11, 28). Single neurons have been shown to use more than one chemical messenger, often choosing a classical transmitter and one or several peptides (29). To understand the integrative processes of the nervous system, it is necessary to map out both the synaptic contacts and the interactions mediated by peptides as well as classical transmitters.

We are particularly interested in the roles of neuropeptides in governing behavioral processes. The gastropod mollusc *Aplysia californica* is a useful model system for these studies due to the numerical simplicity and accessibility of the CNS. Many neurons are readily identifiable based on their size, color, shape, location, and endogenous electrical activity (14, 19). The roles of a number of these cells in neural circuits that govern simple behaviors have been defined using physiological techniques (21, 22, 46, 55).

The most widely studied components of the *Aplysia* CNS are the buccal and abdominal ganglia (Fig. 1). The buccal ganglion is situated on the buccal musculature and mediates a variety of activities associated with feeding (22, 27, 30). The abdominal ganglion governs a number of reflex and fixed action patterns including withdrawal of the gill, inking, and egg laying (18, 21, 22, 45).

Many of the identified *Aplysia* neurons have been shown to synthesize large amounts of specific low molecular weight proteins which are thought to be neuropeptides and their precursors (1, 3, 15, 20, 53, 56). In some cases these peptides have been purified, characterized, and shown to have biological activities (2, 25, 39, 40). Our approach has been to use the techniques of recombinant DNA to isolate genes encoding these prevalent low molecular weight proteins and to study the flow of information from gene expression to the function of the protein product. Using differential screening techniques we have isolated the genes encoding the precursors for peptides expressed in the buccal ganglion cells B1 and B2 (30), the bag cells, atrial gland (46), and abdominal ganglion neurons R3–14 (33), L11 (51), and R2 (44) (Fig. 1).

We have generated antibodies to component peptides of these precursors using either synthetic peptides defined from the sequence of the gene, peptides isolated from *Aplysia* tissue, or commercially available peptides. These antibodies were used to map the positions of immunoreactive cell bodies and processes in the *Aplysia* CNS. Small networks of neurons ranging from as few as 13 to as many as 100 cells react with the various antibodies. The neurons send processes to the

[1] *Abbreviations used in this paper:* BCP, bag cell peptide; CNS, central nervous system; DCV, dense core vesicle; ELH, egg-laying hormone; FMRFamide, PheMetArgPhe-amide; PA-Au, Protein A-coated gold colloid; SCP, small cardioactive peptide.

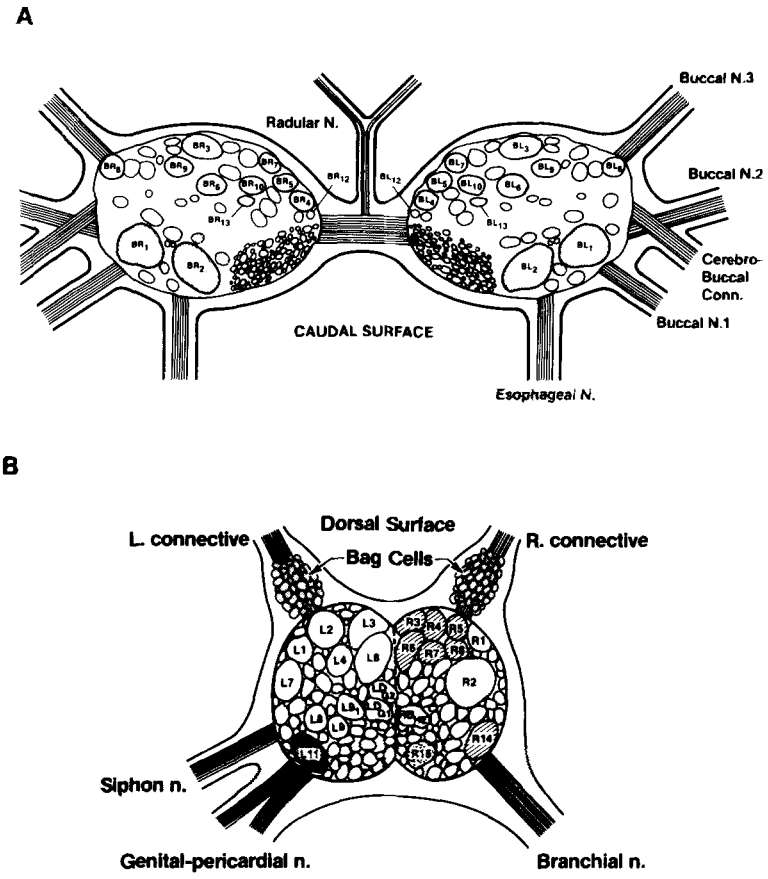


*Figure 1.* Buccal and abdominal ganglia of *Aplysia*. (*A*) The caudal surface of the buccal ganglia is diagrammed, showing the major nerves and identified cells. Cells are identified by a *B* followed by an *L* or *R* for left or right hemiganglia and a number. The shaded neurons are some of the cells which express the gene encoding the small cardioactive peptides *A* and *B*. Neurons B1 and B2 were used in this study. (*B*) The dorsal surface of the abdominal ganglion with identified cells indicated by an *L* or *R* for left or right hemiganglia and an identifying number. The bag cells, R3–8 and R14, L11, and R15 are among the peptidergic cells studied in the report.

neuropile, the connective tissue sheath, or specific peripheral targets such as the heart or the body wall (24, 27, 31, 32, 44, 52).

In this report we present the results of an immunoelectron microscopic study of the subcellular localization of the peptides. Determining the subcellular distribution of the peptides furthers our understanding of their biogenesis and suggests functional roles. The immunoreactivity is largely localized to dense core vesicles (DCVs) and a quantitative analysis of the size distribution of the DCVs is presented. Based on size and morphology, each cell has a characteristic and complex set of granules.

## Materials and Methods

### Tissue

*Aplysia californica* from 50–500 g were obtained live either by expedition or from Sea Life Supply (Sand City, CA) and maintained in a seawater tank until use. Generally, ganglia and atrial glands were removed from the animals and immediately fixed appropriately for analysis.

## Antibodies

The preparation of many of the antibodies used in this study have been previously reported (24, 27, 44, 52). Antisera against PheMetArgPhe-amide (FMRFamide) was generously provided by Dr. Eckard Weber (54). All antisera used were generated in rabbits and separated from the coagulant blood by centrifugation. Further purification was not necessary.

## Electron Microscopy

Neurons used for the vesicle size distribution analysis were fixed in ganglia for 4–6 h in 4% glutaraldehyde, 2% paraformaldehyde, 1% acrolein, 1% dimethyl sulfoxide, 0.3M sucrose in PBS (0.01 M phosphate, 0.15 M NaCl), pH 7.4. After several washes, the neurons of interest were dissected free, and osmicated (2% in PBS) for 2 h. Atrial gland tissue was treated in the same fashion. Excess osmium was removed and tissues stained en bloc with 2% aqueous uranyl acetate for 2 h, then washed in double-distilled $H_2O$, dehydrated stepwise in a graded EtOH series, transferred to propylene oxide, and gradually infiltrated and embedded with Epon-Araldite. Thin (65–70 nm) sections were cut on a diamond knife, mounted on formvar-coated copper grids, and examined and photographed on a Philips 410 transmission electron microscope.

## Immunoelectron Microscopy

*Ultrathin Cryosections.* Ganglia were fixed in 4% paraformaldehyde, 0.7 M sucrose in PBS, pH 7.4, for 4 h, and single neurons were dissected free. These were then fixed overnight in the same fixative, and washed several times. The neurons were then infiltrated with 10% gelatin, and the gelatin hardened; neurons were then fixed in 4% paraformaldehyde/0.7 M sucrose overnight, then infiltrated with 2.3 M sucrose. The neurons were mounted on small stubs and quickly frozen by plunging into liquid Freon. Ultrathin cryosections were cut on glass knives at −110°C in a Reichert FC4 cryo-unit, collected on drops of 2.3 M sucrose, and placed on formvar-coated nickel mesh or slot grids. The excess sucrose and fixative was removed by floating for 10 min in 50 mM $NH_4Cl$ in PBS containing 1.5 g glycine/liter. Grids were transferred to drops of 4% BSA, PBS–glycine for 10 min, to primary antisera diluted 1:100 for 30–60 min, washed three times in PBS–glycine, and transferred to protein A–coated gold colloid of 6 or 10 nm (PA–Au6 or PA–Au10, respectively) for 20–40 min. The PA–Au complexes and gold colloids were prepared using the method of Slot and Geuze (47); PA was obtained from Pharmacia Fine Chemicals (Piscataway, NJ) or Boehringer Mannheim Biochemicals (Indianapolis, IN). The grids were washed several times in PBS–glycine, then for 10 min in 1 M NaCl, then several times in double-distilled $H_2O$ (5, 38). Grids were dried and observed on the Philips 410 transmission electron microscope.

*Lowicryl K4M.* Ganglia and other tissue of interest including atrial glands and components of the *Aplysia* cardiovascular system were fixed in 4% paraformaldehyde, 0.1% glutaraldehyde, 0.1% acrolein, 1% dimethyl sulfoxide, 0.3 M sucrose in PBS, pH 7.4, 4 h–overnight. Excess fixative was cleared for 2 h in 50 mM $NH_4Cl$–PBS, tissues stained en bloc for 2 h with 2% aqueous uranyl acetate, and dehydrated in a graded ethanol series at 20°C to 100%, then gradually infiltrated with Lowicryl K4M resin (Pelco) and polymerized at

−20°C. Thin sections (65–70 nm) were cut and mounted on formvar-coated nickel grids, which were allowed to dry at least 1 h. These were floated on drops of 50 mM $NH_4Cl$ for 10 min, transferred to 4% BSA for 10 min, and reacted with the antisera at 1:100 dilution for 40 min at room temperature. After washing with PBS three times, the grids were transferred to PA–Au as above for 20–30 min, washed in PBS three times, and then $H_2O$ three times, dried 30 min, and stained 10 min with 2% aqueous uranyl acetate. For double-labeling experiments, after the first PA–Au complex, the grids were floated on 0.1 mg/ml PA for 10 min, and then briefly washed; the second antisera and PA–Au complex were reacted in the same way. Gold colloid preparations used in double-labeling experiments were of sufficient homogeneity such that <5% of one size particle could be mistaken for the other; ~20% of our preparations were adequate for these experiments. (See Fig. 5, *D* and *E*, for examples of the preparations). The results of our double-labeling experiments cannot be explained by inhomogeneity of the PA–Au complexes. Appropriate control experiments were performed for both immunoelectron labeling techniques, including: incubation of tissue directly with PA–Au to identify nonspecific absorption; incubation of sections using antisera blocked with its antigen; incubation with antisera followed by unlabeled PA before the PA–Au; incubation with antisera followed by PA–Au preabsorbed with an excess of IgG; and incubation with preimmune sera or a serum recognizing peptides localized to other neurons in place of the primary antisera (5, 38).

## Immunofluorescence

1-μm Lowicryl sections from the same blocks used in the immunoelectron microscopy were dried onto glass slides for 30 min. Primary antisera in a solution containing 0.4% saponin, 2% BSA, 0.1% normal goat serum was applied for 6 h at 4°C; excess was removed by washing several times in PBS, and a secondary goat anti-rabbit fluorescein isothiocyanate conjugate (Miles Laboratories Inc., Elkhart, IN) at a 1:50 dilution in 0.4% saponin, 1% normal goat serum, PBS, and reacted for 2 h at room temperature in the dark. Slides were washed and coverslipped for examination on a Zeiss epifluorescence microscope.

## Digitization of Vesicle Sizes

Electron micrographs were made of random sections of single cells through at least three different levels. Using a Bioquant program (R&M Biometrics, Inc., Nashville, TN), the diameters of single vesicles were measured on a Houston Instruments digitizing tablet. In some cases the areas and perimeters were also measured for the same vesicles. Control for resolution of the digitizing technique was affected by using circles of five sizes covering the range of vesicle sizes encountered, and measuring these diameters repeatedly, but not successively. To control for the possibility of differences in individual cells, we measured the sphere diameters in three individual R14 neurons (data not shown). Single cells were also analyzed for B1–B2, and L11. In all cases, the overall distributions seen in the total histogram were reflected in measurements from individual cells; however, the frequencies at each peak were somewhat variable. Since each single cell histogram consists of only ~200 DCVs, the sampling error is larger, possibly resulting in variable frequencies.

## Estimation of Sphere Diameters

The raw data was grouped into bin sizes of 10 nm. The limit of resolution on the digitizer was 3 nm, and therefore no additional information would be gained by a smaller bin size. Because of the large span of sizes covered by the vesicles in the bag cells and atrial gland, bin sizes of 40 nm (bag cells) and 100 nm (atrial gland) were used. The method of Cruz-Orive (8) was used to transform the data from profile diameters to sphere diameters. This method gives a distribution-free estimate of sphere diameters by taking into account the minimum size profile observable and the capping angle (8). The minimum size cut used was 30 nm to avoid confusing DCVs with other cellular compartments. The capping angle was determined to be 35° using the method suggested by Cruz-Orive (8). The algorithm was implemented on an IBM PC. No dramatic changes in the shape of the histograms was observed because of the transformation, although several of the bin sizes showed significant frequency shifts. This was usually the case when there was a large shift upward between bins. The shift is heightened in the transformed histogram due to the assumption that many of the profile diameters in the smaller bin size were oblique cuts of the immediately higher bin size.

## Gaussian Fits to Histograms

The number of populations in each neuron was estimated from the number of peaks in the histograms, and the shape of the Q–Q plot. Adjusted Q–Q plots (13) were used to estimate starting points for the calculation. A least squared iterative algorithm (13) was then used to determine the best fit. When the number of populations was ambiguous from the histogram and Q–Q plot, then a fit to all of the possible numbers of populations was carried out. A fit with an extra population was only included if it improved the mean squared error by a factor of 2.

# Results

## The Small Cardioactive Peptides A and B ($SCP_A$ and $SCP_B$)

$SCP_A$ and $SCP_B$ are 11- and 9-amino acid–amidated peptides which share the carboxy-terminal 7 amino acids. The SCPs are found in tandem on a single 136-amino acid precursor just after the signal sequence (Fig. 2*A*) (30). The peptides are expressed throughout the CNS; however, 90% of the SCP activity originates from neurons in the buccal ganglion, suggesting that these peptides play a role in feeding behavior (27).

The subcellular distribution of the SCPs was investigated in buccal neurons B1 and B2 (Fig. 2, *B–D*). These cells are easily identifiable on the ventral surface of the ganglion and send processes to the esophagus (Fig. 1*A*) (21, 22, 27). A section through an osmium-stained B1 or B2 neuron reveals the expected organelles including the nucleus, mitochondria, endoplasmic reticulum, and Golgi region (Fig. 2*B*). The characteristic DCVs seen in all of the peptidergic neurons are quite apparent. A histogram of DCV sizes suggests a multimodal distribution with two main peaks centered on 73 ± 15 and 106 ± 16 nm.

Antisera was generated against commercially available synthetic $SCP_B$ coupled to BSA with carbodiamide (27). The antisera was reacted with ultrathin sections of a Lowicryl-embedded B2 soma, followed by washes and a second incubation with protein A coupled to 6-nm colloidal gold (PA–6) (Fig. 2*C*). The gold particles are observed within DCVs, demonstrating localization of the peptide immunoreactivity to these organelles. Few gold particles are seen in the cytoplasm, suggesting that the antibody may not recognize the precursor protein, a common situation with small amidated peptides. Most vesicles contain material which reacts with the antisera; in contrast, another membrane-enclosed organelle, the mitochondrion, displays no label (Fig. 2*C*).

The limit of resolution for the PA–Au technique has been estimated at 16 nm for 3-nm gold particles, based on the size of the PA–Au–IgG complex (38); therefore, gold particles within this distance (or correspondingly greater for larger gold particles) of DCVs probably represent intravesicular antigen recognition. It is likely that for antigen recognition to occur, a vesicle must be cut in such a way that the contents are exposed to the surface which comes into contact with antibody. Therefore, vesicles below the upper surface of the section may appear not to contain peptide (5, 38).

$SCP_B$ immunoreactive DCVs of the same size present in B2 soma are found in processes and terminals innervating the esophagus, salivary gland, and accessory radula closer muscle. A section of Lowicryl-embedded esophagus reacted with anti-$SCP_B$ antisera followed by PA–15 is shown in Fig. 2*D*. The concentration of label is significantly above background in the process displayed.

## FMRFamide

Antisera against the tetrapeptide FMRFamide react specifically with ~100 neurons in the *Aplysia* CNS. These neurons

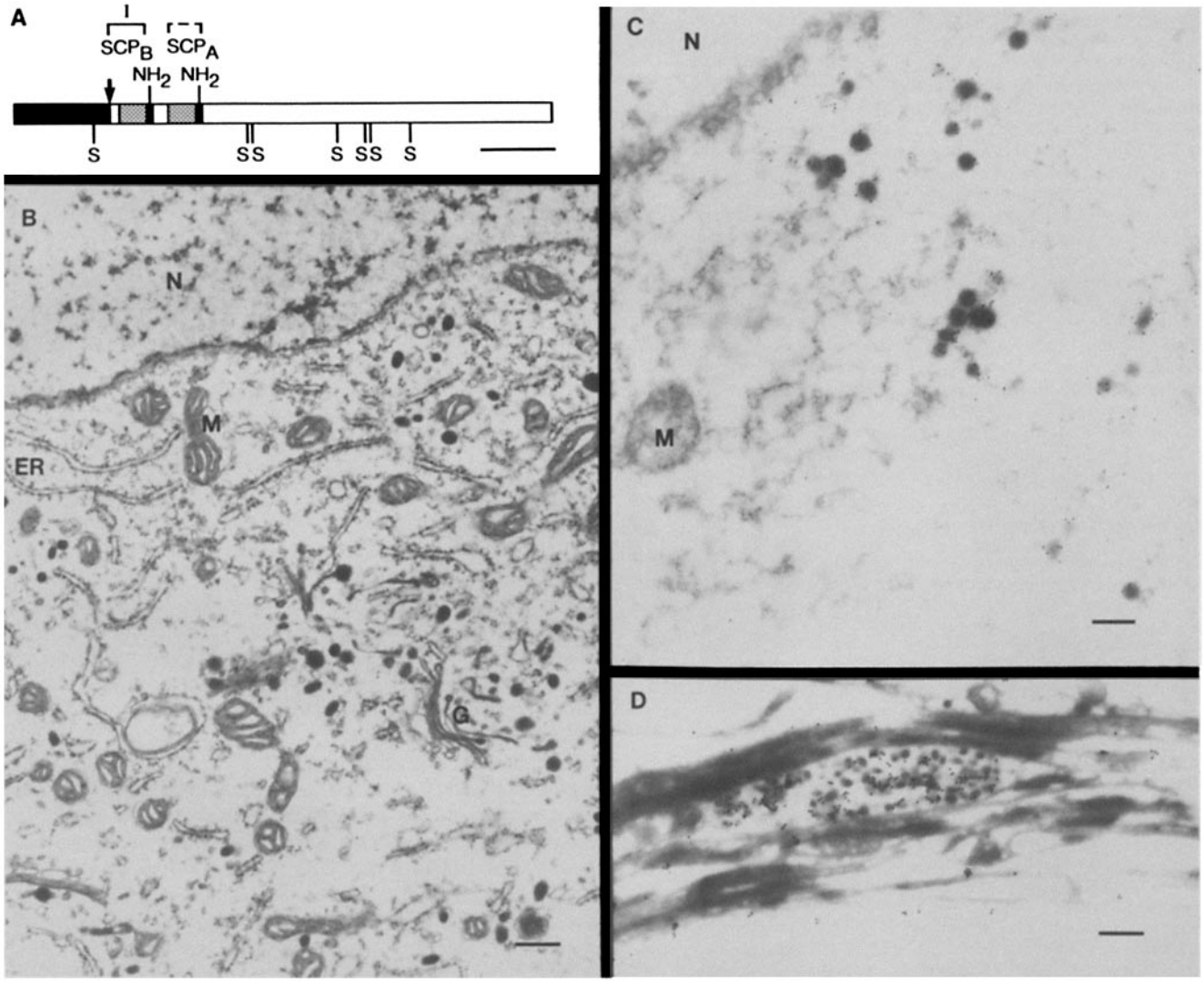


*Figure 2.* Distribution of the small cardioactive peptide B in B1 and B2. (*A*) Schematic representation of the precursor encoding the SCPs. The signal sequence is indicated by the black box and approximate position of signal sequence cleavage by the arrow. The positions of proteolytic cleavage are indicated by the lines; an $NH_2$ above the line indicates carboxy-terminal amidation of the peptide. The homologous regions of $SCP_A$ and $SCP_B$ are indicated by the stippled region. An *S* below the precursor indicates the position of a cysteine. The bracket above the precursor schematic indicates the region used to raise antibodies, in this case $SCP_B$. The dashed bracket indicates a homologous region, $SCP_A$, which is likely to cross-react with the antibody. Bar, 20 amino acids. (*B*) Section of an osmicated B1 or B2 neuron. *N*, nucleus; *M*, mitochondria; *ER*, endoplasmic reticulum; and *G*, Golgi region. DCVs are present in two size classes (see Table I). Bar, 300 nm. (*C*) Lowicryl-embedded B2 neuron section reacted with anti-$SCP_B$ antibody followed by 6-nm colloidal gold coated with protein A. Most of the gold particles are over dense core granules. *N*, nucleus; *M*, mitochondria. Bar, 200 nm. (*D*) Process in Lowicryl-embedded esophagus section, reacted with anti-$SCP_B$ antisera, followed by PA-15. Bar, 400 nm.

include the identified cells R2, LP1, L12, and L13 (44). R2 synthesizes acetylcholine as well as FMRFamide, and sends processes to the body wall where they terminate on mucus-secreting cells (37) (Fig. 1*B*). The precursor encoding FMRFamide gives rise to as many as 19 copies of the tetrapeptide (Fig. 3*A*). The spacer region between the peptides is usually 8 amino acids and quite acidic, resulting in an approximately neutral precursor. Further studies of this unusual precursor are in progress.

Unlike the other neurons investigated in this study, R2 does not contain a large number of dense core granules. The size distribution of vesicle profiles is fit well by a single gaussian curve having a mean diameter of 65 nm (see Fig. 3*B* and Fig. 8, *A* and *B*). Another very rare class of large granules are found to have a mean diameter of 300 nm. Antisera raised against synthetic FMRFamide was reacted with Lowicryl sections of neuron R2. Control experiments to insure the specificity of the reaction included reaction of the antibody with synthetic peptide prior to staining tissue sections or using preimmune sera as the primary antibody (5, 38) (Fig. 3*C*). Fig. 3*D* shows staining of an R2 cell soma. The staining is specific and a large fraction of the particles are over recognizable DCVs as indicated by the arrows. Some particles which appear to be staining above background do not appear in DCVs. There are several possible explanations: some FMRFamide may indeed be free in the cytoplasm; the non-DCV FMRFamide may be a tissue-processing artifact (that is, the peptide may not be adequately fixed in situ); the peptide

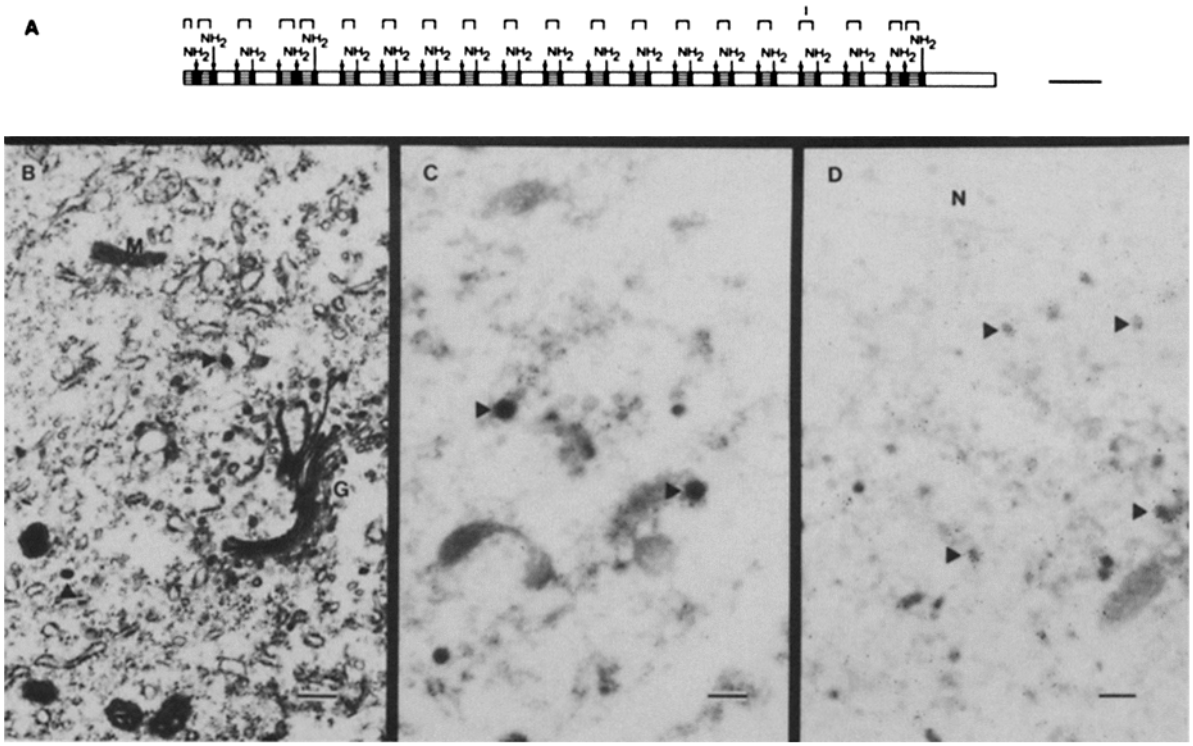


*Figure 3.* Distribution of FMRFamide immunoreactivity in R2. (*A*) Schematic of an FMRFamide precursor. The arrows and lines indicate positions of potential proteolytic cleavages at dibasic or single basic residues respectively; an $NH_2$ indicates amidation. The FMRFamide regions are indicated by the horizontal lines. The brackets above are regions that will react with the antibody used in this study; in this case all of the units are FMRFamide. Bar, 20 amino acids. (*B*) Section of an osmicated R2 soma. *M*, mitochondria; *G*, Golgi region. The arrowheads point to dense core granules. Bar, 300 nm. (*C*) Immunoelectron microscopic staining of the R2 soma reacted with anti-FMRFamide which had first been blocked by incubation with 10 ng/μl of the peptide. The arrowheads indicate DCVs; very few gold particles are seen in the section. Bar, 200 nm. (*D*) Anti-FMRFamide immunoelectron microscopic staining of the R2 soma. PA-6 was used to visualize the antibody. *N*, nucleus. Arrowheads point to dense core granules. Bar, 200 nm.

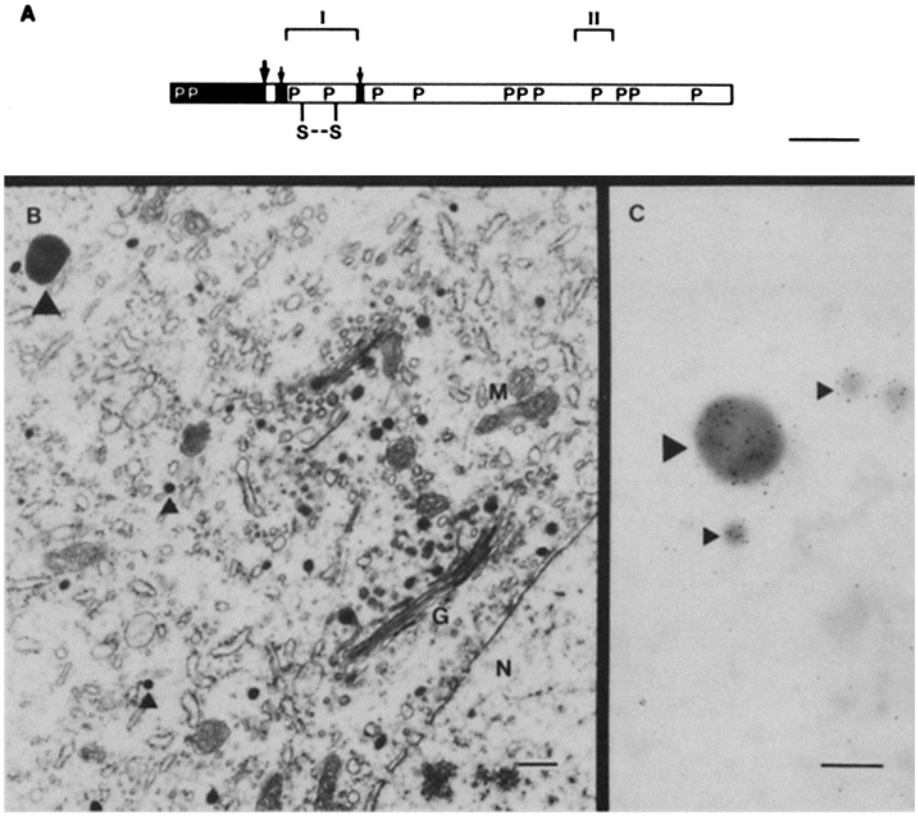


*Figure 4.* Localization of the L11 peptide. (*A*) The L11 peptide precursor. Large and small arrows indicate positions of potential cleavage of the signal sequence and internal proteolytic cleavages, respectively. *S* represents cysteine residues and *P* represents the positions of 13 proline residues. Brackets indicate two regions of the precursor where peptides were synthesized and used to raise antibodies. Antipeptide I was used in this study. Bar, 20 amino acids. (*B*) Section of an osmicated L11 soma. *N*, nucleus; *G* Golgi region; *M*, mitochondria. The arrowheads indicate large and small dense core granules. Bar, 300 nm. (*C*) Cryoultramicrotome section of an L11 cell body reacted with anti-peptide I followed by PA-6. The arrowheads indicate large and small DCV as in *B*. Bar, 200 nm.

may be in other organelles which are not readily discernible in these micrographs.

### *The L11 Peptide*

L11 is a cholinergic neuron located on the left side of the dorsal surface of the abdominal ganglion which sends processes to the body wall below the mantle shelf (Fig. 1 *B*) (21, 22). While no biologically active peptides have yet been identified, a precursor protein specifically expressed in L11 has been characterized (51). A schematic of this proline-rich

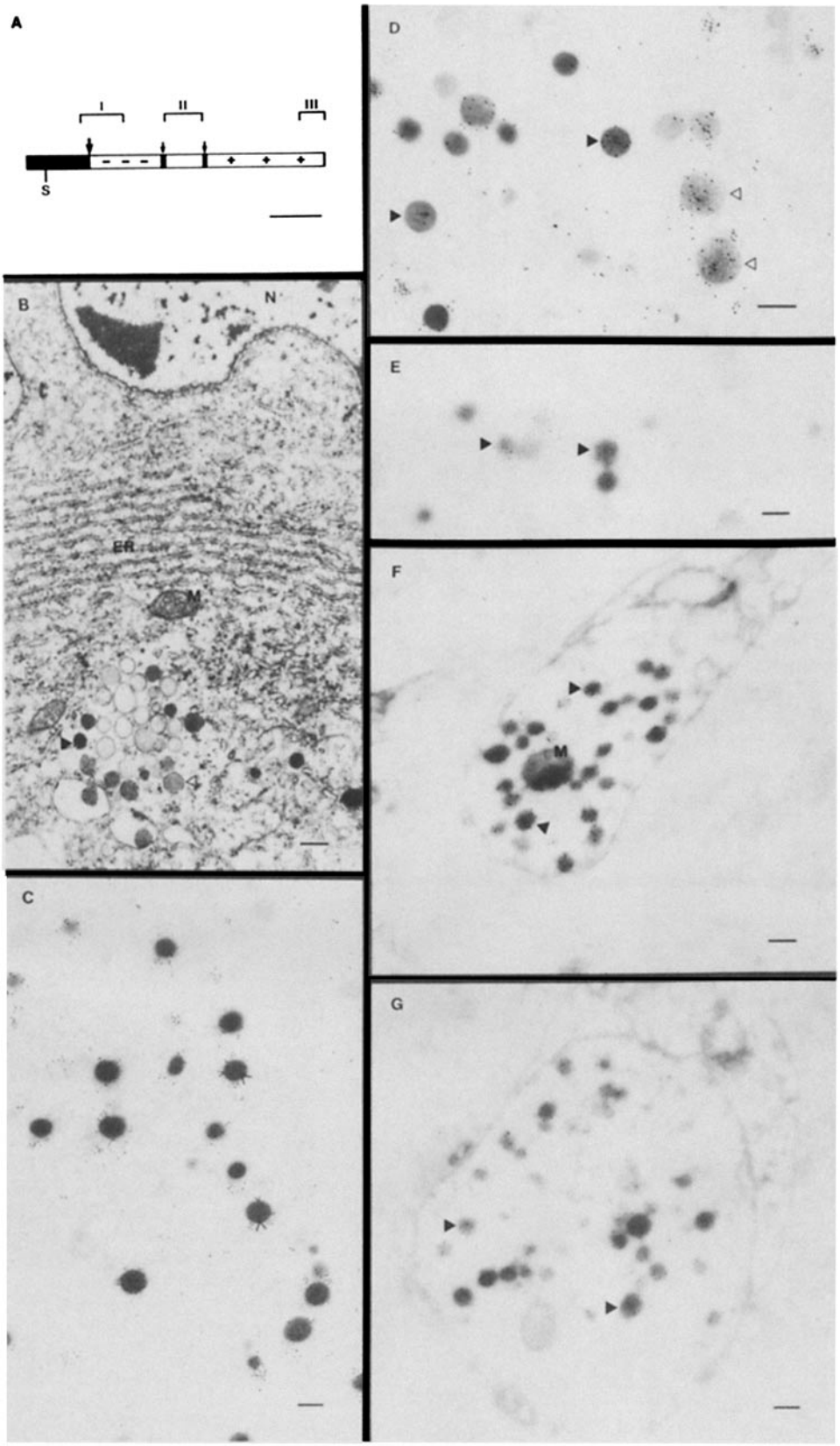


*Figure 5.* Localization of the R14 peptide. (*A*) Schematic diagram of the R14 peptide precursor. Large and small arrows indicate signal sequence and internal proteolytic cleavage sites, respectively. *S* represents a cysteine residue. The + and − symbols denote acidic and basic portions of the precursor. Three peptides, denoted *I*, *II*, and *III*, were synthesized and used to raise antibodies as shown by the brackets above the precursor. Bar, 20 amino acids. (*B*) Section of an osmicated R14 soma. *N*, nucleus; *M*, mitochondria; *ER*, endoplasmic reticulum. The filled in arrowheads indicate DCVs and the open arrowheads indicate granular vesicles. Bar, 300 nm. (*C*) Double-labeling of R14 DCVs. A Lowicryl section of the R14 cell body was reacted with anti-peptide II followed by PA-10. Any unreacted antibody was then blocked with an excess of cold PA and a second antisera, against peptide III, was incubated with the section followed by PA-6. The large arrowheads point to PA-10 and the small arrowheads to PA-6. Bar, 200 nm. (*D*) Lowicryl section of an R14 cell body showing dense (black arrowhead) and granular (white arrowhead) vesicles stained with anti-peptide III followed by PA-10. Bar, 200 nm. (*E*) Cryoultramicrotome section of a right upper quadrant neuron, R3–8, reacted with anti-peptide I followed by PA-6. Arrowheads indicate DCVs. Bar, 200 nm. (*F*) A Lowicryl section of a terminal in the muscle of the anterior aorta. The section was reacted with anti-peptide II followed by PA-6. The arrowheads point to examples of immunoreactive DCVs. *M*, mitochondrion. Bar, 200 nm. (*G*) A Lowicryl section of the branchial nerve reveals a cross section through an R3–14 axon. This section was reacted with anti-peptide II and PA-6. Arrowheads indicate DCVs. Bar, 200 nm.

molecule is shown in Fig. 4*A*. The precursor contains a hydrophobic leader peptide and two pairs of dibasic residues flanking a pair of cysteines.

Sections of an osmicated L11 soma reveal an architecture common to peptidergic neurons: extensive Golgi complex and DCVs. The DCV size distribution is quite complex in that it cannot be fit well by a single gaussian distribution (Table I). This distribution suggests the presence of multiple vesicle size classes as will be discussed later. The large number of clear vesicles observed may reflect the cholinergic nature of this neuron (16, 17). Two peptides have been synthesized and used to raise antibodies (52) (Fig. 4*A*). Electron microscopic labeling studies localize the peptide immunoreactivity to the multiple size classes of DCVs (Fig. 4*C*).

### *The R14 Peptide*

The abdominal ganglion neurons R3–14 are thought to be both glycinergic and peptidergic (35, 41–43). Our light level immunohistochemical studies demonstrated that these cells send processes into the vascularized connective tissue sheath surrounding the ganglion and connectives, and to the efferent vein of the gill at the base of the heart. R14 is anatomically distinct in that it sends immunoreactive processes to other regions of the vasculature including the anterior aorta and the abdominal ganglion artery (24, 34, 36). The peptide precursor is 108 amino acids and is proteolytically processed at three sites including removal of the signal sequence and cleavage of two internal dibasic residues (33) (Fig. 5*A*).

R14 is a large white neuron which is easily identified in the right lower quadrant on the dorsal surface of the ganglion (Fig. 1*B*). The somata contains extensive endoplasmic reticulum, characteristic of a large amount of secretory product biosynthetic activity (Fig. 5*B*). In addition, two morphologically distinct vesicle types, one containing dense and the other granular cores, are seen. Both vesicle types show multimodal size distributions; however, the granular vesicles are somewhat larger than the DCVs. The RUQ neurons (R3–13) are the only other cells in *Aplysia* that express this peptide-encoding gene (33); the distribution of dense core and granular vesicles in these neurons differs from that in R14, having a wider distribution of classes (Table I).

Three peptides have been synthesized, coupled to protein carriers, and used to raise antibodies (24) (Fig. 5*A*). Immunoelectron microscopic studies demonstrate that each of the antibodies recognize antigen in the dense core and granular vesicles of both R14 and the RUQ (R3–13) neurons, as shown in Fig. 5, *D* and *E*. The use of Lowicryl-embedded tissue greatly improves the morphology of the tissue, allowing a clear visualization of the granular vesicles (Fig. 5*D*). A number of gold particles are seen in the cytoplasm outside the granules. This staining is above background and may be attributed to precursor in the secretory pathway; however, Lowicryl sections with well-preserved membranes suggests that some of the immunoreactivity may be outside the endoplasmic reticulum, Golgi region, or granules.

To conclusively demonstrate the co-localization of all three regions of the R14 precursor, a series of double-label experiments were conducted. An example is shown in Fig. 5*C*; in this case, a Lowicryl section of neuron R14 was reacted with antisera against peptide II followed by PA–Au6, blocked with excess PA, reacted with antisera against peptide III followed by PA–Au10, and examined. Both small and large gold particles are visible in the majority of DCVs. Different combinations of primary antisera demonstrate co-localization of all regions of the precursor. All possible permutations of antisera, PA–Au, and sequence of reaction were examined, and each demonstrated the same result. Further control experiments included blocking one or both antisera with peptide or using normal rabbit sera as the primary antibody to determine background (5, 38).

We have examined the distribution of R14 peptide immunoreactive DCVs in the nerves exiting the abdominal ganglion as well as peripheral targets. In Fig. 5*F*, a terminal in the muscle of the anterior aorta is seen to contain immunoreactive DCVs. Fig. 5*G* shows a cross section through a large axon in the branchial nerve which also contains immunoreactive DCVs.

### *The Egg Laying Hormone (ELH) Gene Family*

Oviposition and the associated behavior is governed by a family of five neuropeptide genes expressed in an exocrine gland and the CNS (18, 26, 31, 39, 46, 49). The genes are

*Table I. Calculated Frequencies and Sizes for Vesicle Populations in Aplysia Neurons Compared to Predicted Quantal Vesicle Sizes*

| Source | N | Mean squared error | Quantal vesicle size | | | | | | | |
|---|---|---|---|---|---|---|---|---|---|---|
| Predicted (6) | | | 69 | 95 | 120 | | 172 | | | + |
| Predicted (12) | | | 70 | 95 | 120 | 145 | 170 | 195 | 220 | + |
| Atrial gland | 374 | 6.7 | | | | | | | | 100% 300–2500 |
| B1-B2 | 1222 | 5.9 | 26% 73 ± 15 | 15% 87 ± 15 | 48% 106 ± 16 | 11% 148 ± 16 | | | | |
| Bag cells | 840 | 4.1 | | | 44% 114 ± 16 | | 46% 159 ± 20 | | | 10% 240–600 |
| L5 | 420 | 3.2 | 55% 81 ± 16 | 42% 105 ± 18 | | 3% 155 ± 6 | | | | |
| L6 | 633 | 2.6 | 85% 75 ± 16 | | 10% 115 ± 18 | 5% 136 ± 18 | | | | |
| L10 | 594 | 2.7 | 38% 75 ± 14 | | 55% 111 ± 17 | | 7% 158 ± 16 | | | |
| L11 | 1140 | 2.8 | 72% 77 ± 19 | | 22% 110 ± 15 | 6% 153 ± 15 | | | | |
| L12 | 493 | 6.4 | | 48% 88 ± 13 | 40% 119 ± 17 | 12% 152 ± 25 | | | | |
| L13 | 555 | 2.2 | 23% 68 ± 22 | 40% 86 ± 10 | 26% 114 ± 9 | 6% 138 ± 4 | 5% 158 ± 16 | | | |
| R2 | 570 | 5.9 | 95% 65 ± 21 | | | | | | | 5% 240–400 |
| R14 DCV | 604 | 6.7 | | | 37% 126 ± 15 | | 49% 163 ± 15 | 14% 208 ± 20 | | |
| R14 GR | 530 | 5.3 | | | | 40% 144 ± 16 | 32% 174 ± 12 | 14% 200 ± 4 | 14% 231 ± 12 | |
| R15 DCV | 720 | 2.8 | 11% 64 ± 8 | 48% 100 ± 14 | 34% 132 ± 16 | | 7% 169 ± 7 | | | |
| R15 GR | 745 | 3.2 | 19% 79 ± 10 | | 43% 110 ± 13 | 22% 147 ± 13 | 13% 176 ± 17 | | 7% 225 ± 35 | |
| RUQ DCV | 470 | 5.1 | 13% 73 ± 16 | | 23% 119 ± 16 | 19% 138 ± 25 | 20% 163 ± 18 | 25% 199 ± 20 | | |
| RUQ GR | 300 | 8.2 | | | | 24% 153 ± 1 | 31% 184 ± 6 | 9% 206 ± 4 | 21% 224 ± 12 | 15% 278 ± 30 |

All sizes are in nanometers; *N* is the number of vesicles measured for each cell.

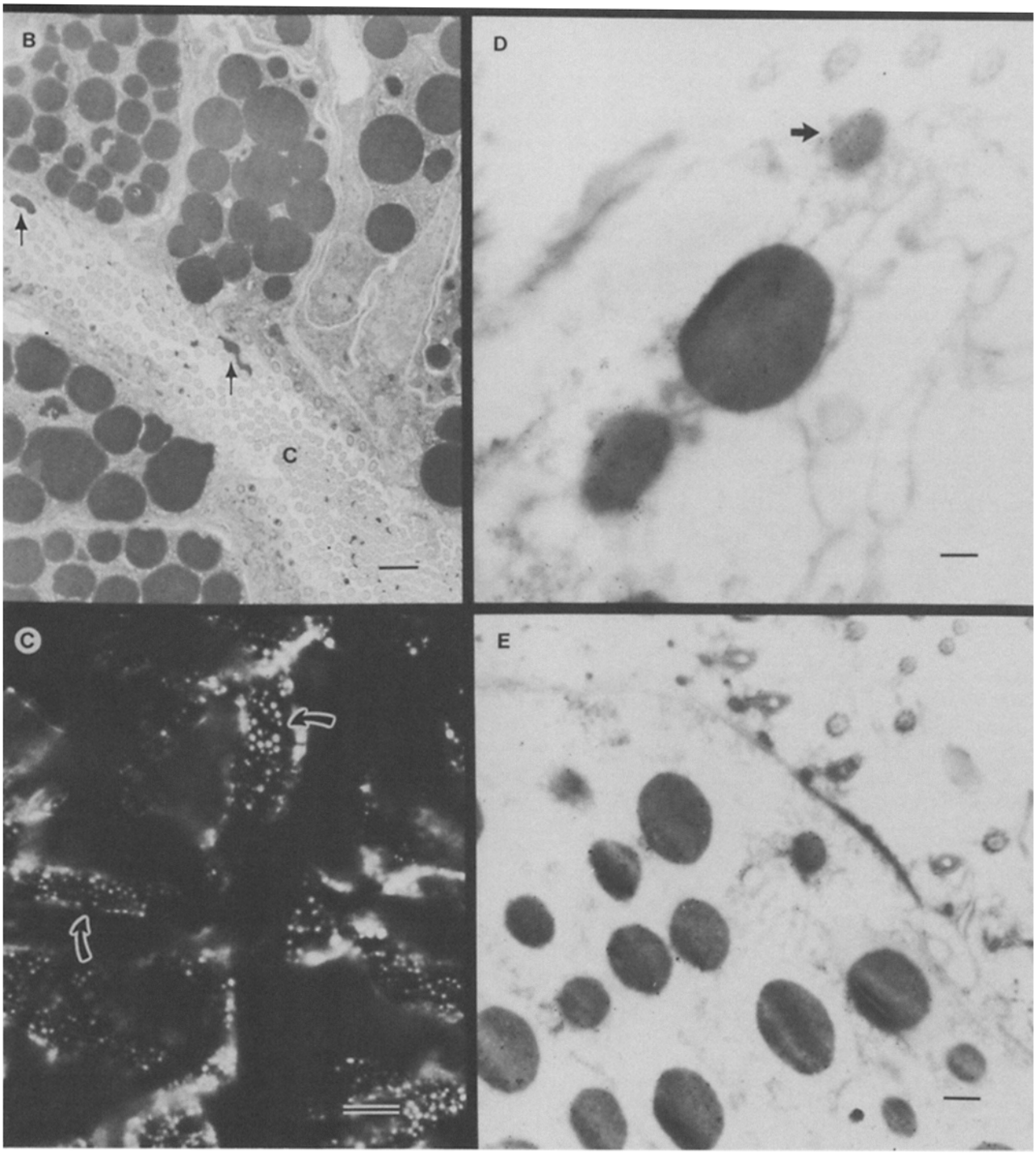
A
II
I
β γ δ
α
ELH
NH2
acidic
S S
I
peptide A
NH2
NH2
S S
S S
B
C
D
C
E

90% homologous, yet due to the location of a few key amino acid substitutions, different sets of related peptides are cleaved from the precursor proteins (45) (Fig. 6*A*).

***The Atrial Gland.*** The atrial gland is situated at the distal end of the hermaphroditic duct at the gonopore. The gland releases its contents into the lumen of the duct, defining the mode of secretion as exocrine. An example of the class of precursor expressed in the atrial gland is illustrated in the lower part of Fig. 6*A*. The precursor gives rise to a 34-amino acid hormone, peptide A, and a molecule related to ELH. A similar precursor (not shown) gives rise to a hormone called peptide B which is homologous to peptide A at 30 of 34 positions. While the precise function of the gland is not known, two hypotheses for the function of the peptides have been put forth. First, Strumwasser and his colleagues (48) has suggested that peptides A and/or B released from the gland initiate a bag cell discharge eventually resulting in an egg-laying episode. Alternatively, behavioral studies suggest the frequency of mating is increased by atrial gland extracts and therefore the peptides may act as pheromones coordinating the actions of individuals within the species (50).

The gland consists of large secretory cells surrounded by ciliated capping cells. The secretory cells contain very large DCVs which are up to 2 $\mu$m in diameter (2) (Fig. 6*B*). These granules are visible in the light microscope when Lowicryl tissue sections are stained with antisera against peptide A or peptide B and a fluorescent secondary antibody. Immunogold labeling using antisera directed against peptide A also demonstrates the presence of the peptide in the vesicles (Fig. 6, *D* and *E*). Antibodies against ELH also stain the granules; however, the reaction is weaker than when antisera against peptide A is used.

***The Bag Cells.*** The major site of ELH gene expression in the CNS is the bag cells, although there are many other immunoreactive neurons (32). There are ~800 bag cell neurons in two clusters on the rostral side of the abdominal ganglion. The cells are electrically coupled and fire a 20–30-min train of action potentials called the afterdischarge during each egg-laying event (18). The precursor expressed in the bag cells encodes a number of potential peptide hormones and transmitters. ELH has been shown to have a host of activities on central neurons and peripheral tissues (26, 39, 40). Another set of candidate peptides, $\alpha$-, $\beta$-, $\gamma$-, and $\delta$-bag cell peptides (BCPs) are contained in the same precursor. The $\alpha$-BCP has actions on abdominal ganglion neurons, largely as a short duration inhibitory transmitter (39).

The bag cells have a complex distribution of DCVs which falls into three discrete size classes (Fig. 7*B*, Fig. 8, *E* and *F*, and Table I). Two biologically active peptides from the ELH precursor have been used to raise rabbit antibodies, the 36-amino acid ELH and the 9-amino acid $\alpha$-BCP (Fig. 7*A*). Micrographs of two Lowicryl sections reacted with anti-ELH and anti-$\alpha$-BCP antisera followed by PA–Au6 are shown in Fig. 7, *C* and *D*. Almost all of the gold particles are associated with DCVs in both cases. Double-label experiments as described for R14 were performed on bag cell sections using anti-ELH and anti-$\alpha$-BCP antisera (Fig. 7*E*). The experiments demonstrate that many vesicles contain both ELH and $\alpha$-BCP immunoreactivity.

Bag cell processes extend rostrally along the pleural abdominal connective to the head and caudally into the connective tissue sheath which surrounds the ganglion (14). Release of bag cell products into the sheath delivers the peptides both to central neurons and the circulation for distribution to distant targets. Rostral and caudal sheath were processed in Lowicryl and examined for immunoreactivity. In Fig. 7*F*, a portion of the rostral sheath is shown to contain a large number of anti-ELH immunoreactive DCVs. The largest size DCVs are not seen in the processes suggesting that these peptide-containing organelles are soma specific.

## *DCV Size Distribution*

Sections of osmicated neuronal cell bodies were photographed at three different levels, often through multiple cells, and the diameter of the DCVs were measured. The raw data was grouped into either 10-nm or 40-nm bin sizes and the method of Cruz-Orive (8) was used to transform the measured profile diameters into sphere diameters.

The histograms generated for the sphere diameters tended to be complex, suggesting the existence of multiple size classes of vesicles in some of the neurons. To further examine this issue Q–Q plots (13) were constructed from the histogram in order to separate possible mixtures of normal distributions. Using a least squared iterative algorithm with starting values generated from adjusted Q–Q plots (13), a best fit to the histograms for each neuron was calculated (Table I).

The R2 DCV sphere diameter histogram (excluding the rare very large DCVs) reflects a single component, normally distributed, with a mean of 65 ± 21 nm (Fig. 8, *A* and *B*). None of the other sphere diameter histograms could be fit by a single normal distribution. An example of one of these complex distributions is seen in the histogram of R14 DCV sphere diameters (Fig. 8*C*). The histogram displays a marked multimodality. The lines in the Q–Q plot corresponding to

*Figure 6.* Immunoelectron microscopic localization of peptides in the atrial gland. (*A*) The ELH and peptide A precursors. The sequences are 90% homologous and the dashed lines between the precursors indicate the positions of insertions or deletions. The large arrows, small arrows and lines indicate positions of signal sequence cleavage and proteolytic processing sites at dibasic or single basic residues, respectively, Some of the known peptides are labeled including ELH, peptide A, the acidic peptide, and the $\alpha$-, $\beta$-, $\gamma$-, and $\delta$-BCPs. The peptide B precursor is similar to the peptide A precursor. In this series of experiments anti-peptide A, B and ELH antibodies were used. Anti-ELH cross-reacts with the homologous region in the peptide A and B precursors. Anti-peptide A or B cross-reacts with the homologous region in the ELH precursor (asterisks) as denoted by the dashed brackets above the schematic. Bar, 20 amino acids. (*B*) Section through an osmicated atrial gland showing the secretory cells which contain large DCVs. *C* denotes the cilia of the capping cells which border the exocrine cells. Arrow indicates dense material in lumen, probably representing a large secreted DCV. Bar, 1 $\mu$m. (*C*) Light micrograph of a Lowicryl-fixed section of the atrial gland stained with anti-peptide A followed by goat anti-rabbit coupled to fluorescein isothiocyanate. The arrows point to regions of immunoreactive granules. Bar, 5 $\mu$m. (*D*) Lowicryl section of the atrial gland reacted with anti-peptide A followed by PA-6. The arrow indicates a section of a granule which may be in the process of secretion. Bar, 200 nm. (*E*) Same as *D*, with PA-15. Bar, 300 nm.

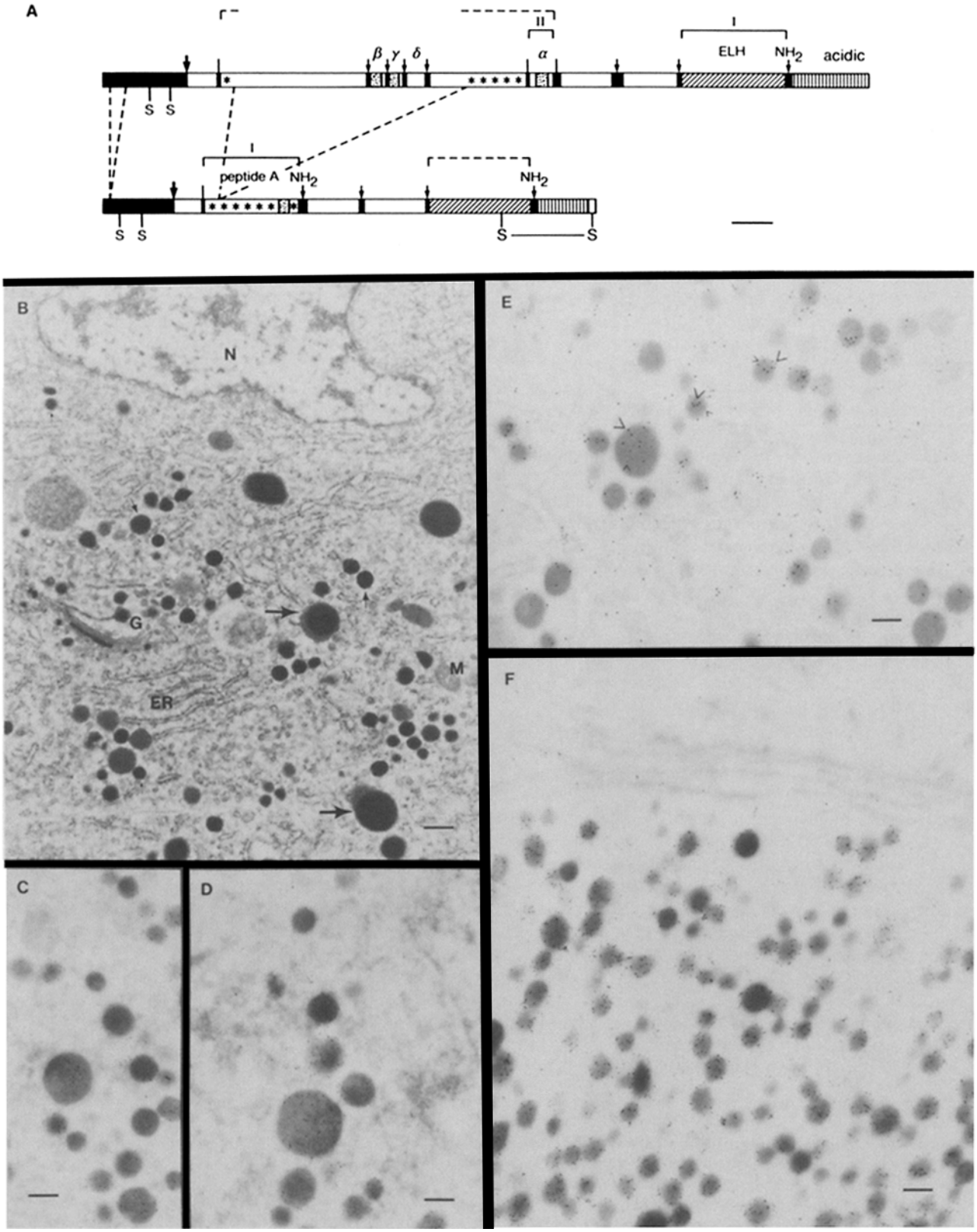


*Figure 7.* EM immunohistochemistry of the bag cells. (*A*) Same as in Fig. 6*A*. In this study, antibodies directed against ELH, region I, and α-BCP, region II were used. α-BCP homologous regions are indicated by the stippled regions in the ELH and peptide A precursors. (*B*) Micrograph of an osmicated bag cell body. *N*, nucleus; *M*, mitochondria; *ER*, endoplasmic reticulum; *G*, Golgi region. The three arrows indicate examples of vesicles belonging to the three different size classes. Bar, 300 nm. (*C*) Section of a bag cell soma reacted with anti-ELH followed by PA-6. Bar, 200 nm. (*D*) Section of a bag cell soma reacted with anti-α-BCP followed by PA-6. Bar, 200 nm. (*E*) Double label of bag cell DCVs. The experiment was done essentially as described for R14. The PA-6 (small arrowheads) represents ELH immunoreactivity and the PA-10 (large arrowheads) represents α-BCP reactivity. Bar, 200 nm. (*F*) Lowicryl section through the pleural abdominal connective sheath reveals a bag cell process containing ELH immunoreactive DCVs. Bar, 200 nm.

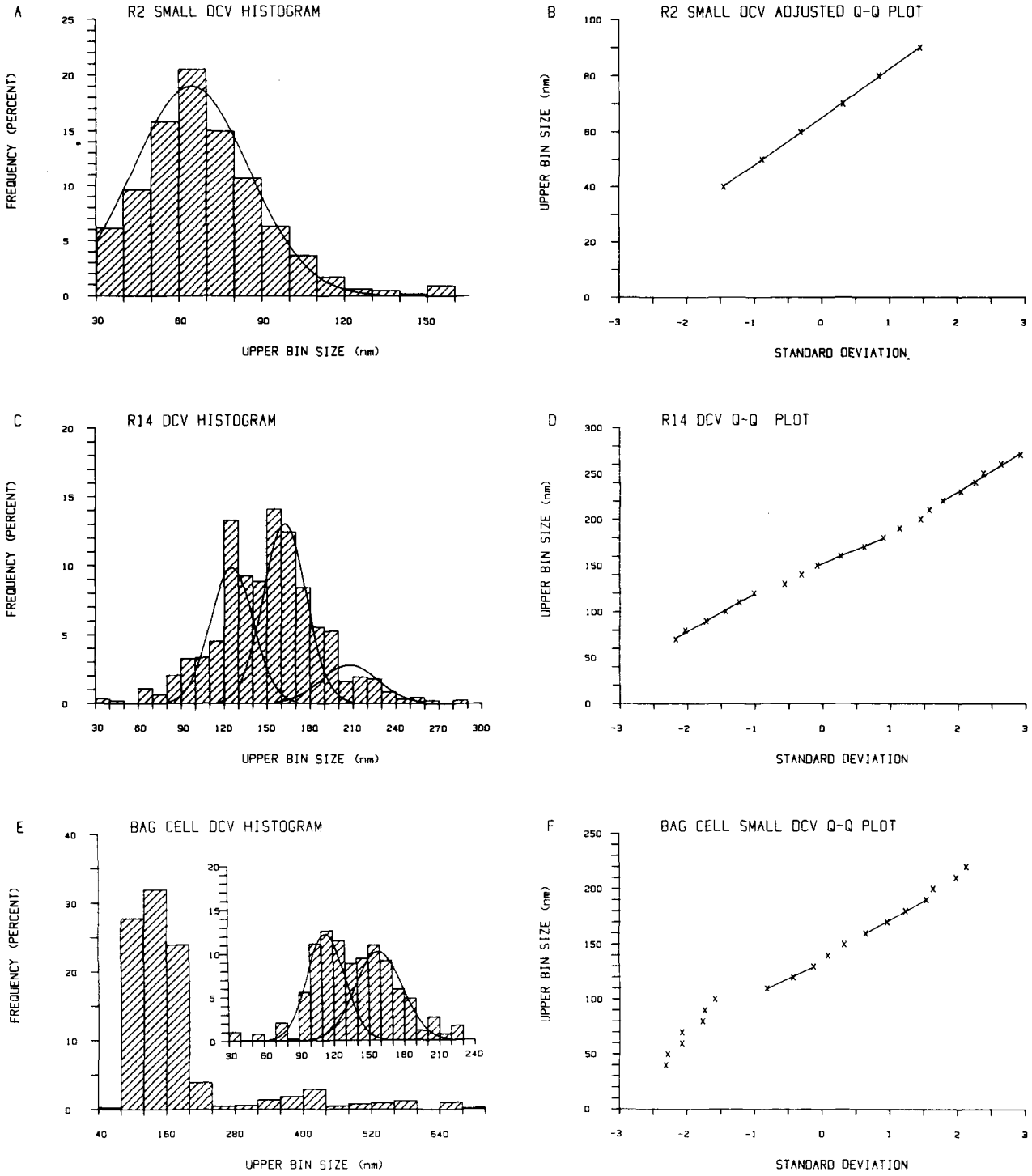


*Figure 8.* DCV size distributions for R2, R14, and the bag cells. (*A*) Estimated sphere diameters for R2 DCVs in the range of 30 to 130 nm. Larger DCVs were measured, but are not shown on this graph. The fitted gaussian has a mean of 65 ± 21 nm. (*B*) Q–Q plot for *A* adjusted to include the range of 30 to 100 nm. The line is a least squares fit to the points shown ($r = 0.9998$). (*C*) Estimated sphere diameters for R14 DCVs. The fitted gaussians described in Table I for the R14 DCVs have means of 126 ± 15, 163 ± 15, and 208 ± 20 nm. (*D*) Q–Q plot for the data in *C*. The lines are least squared fits for the points they cover. These are the regions corresponding to the unmixed portions of the histogram in *C*. (*E*) Bag cell DCVs sphere diameters with a bin size of 40 nm; inset is a histogram of the smaller DCVs with a bin size of 10 nm. In the 40-nm bin size histogram, the large DCVs are overrepresented so that their population distribution could be seen. On micrographs where both vesicle types were counted, large DCVs (>240 nm) represented 5–10% of the vesicles seen. The two gaussians fit to the inset are the best fit from Table I, having means of 114 ± 16 and 159 ± 20 nm. (*F*) Q–Q plot of the data in the inset of *E*. Again, the straight lines represent the unmixed populations separated by a region where the populations are mixed.

the unmixed portions of the populations are shown in Fig. 8 *D*.

A third example is seen in Fig. 8 *E* where the bag cell DCVs are analyzed. In the histogram, the profiles are initially grouped into 40-nm bin sizes to reveal the larger population of vesicles between 250 and 600 nm. These large profiles are only 5–10% of the number of vesicles; however, because of their large size account for up to 50% of the DCV volume in the soma. If one looks more closely at the smaller vesicles by grouping them into 10-nm bin sizes, a clear bimodal distribution is seen (inset, Fig. 8 *E*). The Q–Q plot has two lines corresponding to each of the populations with a mixing region in between the two lines. The region of the Q–Q plot preceding the line is made up of very few vesicles, and this may explain its irregularity. Alternatively, there may be a very small population of small vesicles in the bag cells; the end of the line deviates because of the emerging presence of the very large DCVs. The estimated vesicle diameter was fit to two gaussians using the least squared iterative algorithm with starting estimates from the adjusted Q–Q plot. The fit is a good one (mean squared error = 4.5) and reveals two populations of roughly equal representation: 114 ± 16 nm and 159 ± 18 nm.

There have been reports that the formation of vesicles is physically constrained to certain sizes (6, 7). In these studies, Bont and co-workers showed that vesicles formed by ultrasonic disruption of membranes were formed in quantal sizes. In Table I we have compared the predicted quantal sizes to those determined from the measurements in this study, and to a theoretical model of vesicle sizes (12). The data fit the model rather well, suggesting vesicle formation in vivo may also be subject to physical constraints.

L5, L6, L10, L11, and L12 all have a very similar pattern of vesicle sizes (Table I). The major difference between these neurons is the frequency of the major populations. For instance, the smaller population makes up 85% of L6 DCVs but only 38% of the DCVs in L10. B1–B2 and L13 show a more complex pattern which could not be fit well until a fit of 4 gaussians was attempted. The theory of Bont predicts four vesicle size classes in the range covered by these neurons (see Table I). Bag cells, R14, R15, and RUQ all contain larger vesicles than the other neurons.

## *Discussion*

Gene products expressed in subsets of reproducibly identifiable *Aplysia* neurons are localized in specific classes of DCVs in the soma, processes, and terminals. *Aplysia* is an excellent model system for an integrative approach that allows us to determine the function of neuroactive peptides and to relate the actions of identified cells to simple behaviors. We are beginning to understand how complex neuronal systems function. Additionally, these neurons offer an opportunity to study regulated protein secretion (23) and the significance of multiple transmitter and vesicle types in *Aplysia* neurons.

We have shown that a number of candidate neurotransmitters are contained in DCVs of *Aplysia* neuronal cell bodies and processes as well as in the exocrine atrial gland. Vesicular localization of the peptide products is consistent with their functioning as extracellular messengers. The vesicles provide a mechanism whereby molecules are packaged into discrete quanta, transported to appropriate terminals, and stored until they are required for signaling. Fusion of vesicular membranes with presynaptic terminals allows release of chemical messengers that range from small molecules such as acetylcholine to larger peptides.

Previous studies have implicated acetylcholine as a transmitter in R2, B2, and L11 (16, 17). Acetylcholine is generally stored in small (~40–80 nm) clear vesicles; consistent with this hypothesis, neurons B2, R2, and L11 have a large number of these vesicles. It is not known whether acetylcholine is packaged into DCVs in these cells. Our data suggest that the peptides are not found in clear vesicles; it thus appears likely that these neurons use two different transmitters which are packaged into separate vesicle populations. This situation would potentially allow differential transport and/or release of the different vesicle populations, each containing a unique transmitter. Evidence for differentially regulated vesicle populations has been suggested in other cell types (23); sorting is likely to be dependent on differences in vesicle-associated antigens.

Neurons R3–14 are thought to be glycinergic as well as peptidergic; free glycine has been shown to be packaged in DCVs and transported to terminals (35, 41, 42, 43). While further co-localization studies are necessary before any firm conclusions can be made, the best interpretation of the current data is that glycine and the peptides are packaged in the same granules. This organization does not have the degrees of freedom found in the cholinergic systems and suggests co-release under all circumstances.

Peptides A and B as well as ELH immunoreactive material is localized in the large dense core granules of the atrial gland. The function of these granules is not entirely clear; however, the exocrine mode of secretion suggests a role as pheromones mediating mating activities between individuals (50). The bag cell granules contain immunoreactivity to more than one biologically active peptide, ELH and the $\alpha$-BCP. These molecules are therefore probably released and may act as a peptide co-transmitter system during egg laying in *Aplysia*.

The data support the hypothesis that DCVs are synthesized in quantal sizes. The sizes and the ratio of the different size classes varies from cell to cell and the mechanisms controlling this process are not understood. It is curious that R2, which expresses the gene with the highest molar ratio of peptide to precursor, the FMRFamide precursor, contains the smallest DCVs. The bag cells, which express the most complicated precursor, have a set of very large granules which we have shown are immunoreactive with antisera against two peptides derived from the precursor. These observations suggest a coupling of the DCV contents, function, and size of the granule. The regulation of the amount of transmitter released may in part be controlled by vesicle size which in turn determines the number of molecules per quanta. It is possible that the peptide precursor itself determines vesicle and thus quantal size. Alternatively, each cell may control vesicle size independently of the peptide precursor synthesized.

We have shown that several neuropeptides are transported in DCVs away from cell soma. $SCP_B$ is present in processes and terminals in components of the feeding system including the esophagus, salivary glands, and accessory radula closer muscle, where it is associated specifically with DCVs. The R14 peptide is contained in DCVs in processes innervating the cardiovascular system; it may directly affect these tissues,

and also has the potential to be carried in the hemolymph to act as a circulating hormone. Furthermore, we have observed ELH immunoreactive DCVs in bag cell processes that extend rostrally along the pleural abdominal connective. Only the smaller DCVs are observed in these processes, suggesting the large DCV class serves a soma-specific function as sites of storage, processing, or turnover.

Molecular genetic, biochemical, and physiological studies in conjunction with the cellular studies described here are generating an understanding of the biogenesis of peptide messengers in the *Aplysia* nervous system. Because neurons must carefully regulate when and where they secrete specific substances, further studies of these cells will provide insight into mechanisms of transport, sorting, and differential exocytosis.

The authors are grateful to Frances Thomas for expert technical assistance; Eve Reaven for graciously allowing us to use her image analysis system; Anne Mahon, Ron Taussig, Rashad-Rudolf Kaldany, Malladi Shyamala, and Eckard Weber for antisera; Michael Bastiani for advice and criticism of experiments and the manuscript; and Corey Goodman and Jack McMahan for critically reading the manuscript.

T. Kreiner is a graduate student in the Neurosciences program supported by a National Science Foundation fellowship. W. Sossin is a graduate student in Biological Sciences supported in part by an MRC studentship. This research was supported by a grant to R. H. Scheller from the National Science Foundation. R. H. Scheller is a Klingenstein Fellow in the Neurosciences, and a McKnight Foundation Scholar.

Received for publication 5 August 1985, and in revised form 6 November 1985.

### *References*

1. Arch, S. 1972. Biosynthesis of the egg-laying hormone in the bag cell neurons of *Aplysia californica*. *J. Gen. Physiol.* 60:102–119.

2. Arch, S., T. Smock, R. Gurvis, and C. McCarthy. 1978. Atrial gland induction of the egg-laying response in *Aplysia californica*. *J. Comp. Physiol.* 128:67–70.

3. Aswad, D. 1978. Biosynthesis and processing of presumed neurosecretory proteins in single identified neurons of *Aplysia californica*. *J. Neurobiol.* 9:267–284.

4. Deleted in press.

5. Bendayan, M. 1984. Protein A-gold electron microscopic immunocytochemistry: methods, applications, and limitations. *J. Electron Microsc. Tech.* 1:243–270.

6. Bont, W. S., J. Boom, H. P. Hofs, and M. DeVries. 1977. Comparison between the sizes of granular vesicles in intact cells and vesicles obtained by fragmentation of biomembranes. *J. Membrane Biol.* 36:215–232.

7. Bont, W. S. 1978. The diameters of membrane vesicles fit in geometric series. *J. Theor. Biol.* 74:361–375.

8. Cruz-Orive, M. 1983. Distribution-free estimation of sphere size distribution from slabs showing overprojection and truncation, with a review of previous methods. *J. Microscopy.* 131:265–290.

9. Docherty, K., and D. F. Steiner. 1982. Post-translational proteolysis in polypeptide hormone biosynthesis. *Annu. Rev. Physiol.* 44:625–638.

10. Deleted in press.

11. Eisenstadt, M., J. E. Goldman, E. R. Kandel, H. Koike, J. Koester, and J. H. Schwartz. 1973. Intrasomatic injection of radioactive precursors for studying transmitter synthesis in identified neurons of *Aplysia californica*. *Proc. Natl. Acad. Sci. USA.* 70:3371–3375.

12. Fishman, S. N., and V. A. Krongauz. 1983. A vesicle formation model based on an analogy to quasi-crystals. *Speculations in Science and Technology.* 6:349–352.

13. Fowlkes, E. B. 1979. Some methods for studying the mixture of two normal (lognormal) distributions. *Journal of the American Statistical Association.* 74:561–575.

14. Frazier, W. T., E. R. Kandel, I. Kupfermann, R. Waziri, and R. E. Coggeshall. 1967. Morphological and functional properties of identified neurons in the abdominal ganglion of *Aplysia californica*. *J. Neurophysiol.* 30:1288–1351.

15. Gainer, H., and Z. Wollberg. 1974. Specific protein metabolism in identifiable neurons of *Aplysia californica*. *J. Neurobiol.* 5:243–261.

16. Giller, E., Jr., and J. H. Schwartz. 1971. Choline acetyltransferase in identified neurons of abdominal ganglion of *Aplysia californica*. *J. Neurophysiol.* 34:93–107.

17. Giller, E., Jr., and J. H. Schwartz. 1971. Acetylcholinesterase in identified neurons of abdominal ganglion of *Aplysia californica*. *J. Neurophysiol.* 34:108–115.

18. Heller, E., L. K. Kaczmarek, M. W. Hunkapiller, L. E. Hood, and F. Strumwasser. 1980. Purification and primary structure of two neuroactive peptides that cause bag cell after discharge and egg-laying in *Aplysia*. *Proc. Natl. Acad. Sci. USA.* 77:2328–2332.

19. Kaldany, R-R., J. R. Nambu, and R. H. Scheller. 1985. Neuropeptides in identified *Aplysia* neurons. *Annu. Rev. Neurosci.* 8:431–455.

20. Kaldany, R-R., J. T. Campanelli, M. Schaefer, M. Shyamala, and R. H. Scheller. 1985. Low molecular weight proteins of *Aplysia* neurosecretory cells. *Peptides (NY).* In press.

21. Kandel, E. R. 1976. *The Cellular Basis of Behavior.* W. H. Freeman & Co., San Francisco. 727 pp.

22. Kandel, E. R. 1979. *Behavioral Biology of Aplysia.* W. H. Freeman & Co., San Francisco. 463 pp.

23. Kelly, R. B. 1985. Pathways of protein secretion in eukaryotes. *Science (Wash. DC).* 230:25–32.

24. Kreiner, T., J. Rothbard, G. K. Schoolnik, and R. H. Scheller. 1984. Antibodies to synthetic peptides defined by cDNA cloning reveal a network of peptidergic neurons in *Aplysia*. *J. Neurosci.* 4:2581–2589.

25. Krieger, D. T. 1983. Brain peptides: what, where, and why? *Science (Wash. DC).* 222:975–985.

26. Kupfermann, I. 1970. Stimulation of egglaying by extracts of neuroendocrine cells (bag cells) of abdominal ganglion of *Aplysia*. *J. Gen. Physiol.* 67:113–123.

27. Lloyd, P. E., A. C. Mahon, I. Kupfermann, J. L. Cohen, R. H. Scheller, and K. Weiss. 1985. Biochemical and immunocytochemical localization of molluscan small cardioactive peptides in the nervous system of *Aplysia californica*. *J. Neurosci.* 4:1851–1861.

28. Loh, Y. P., M. J. Brownstein, and H. Gainer. 1984. Proteolysis in neuropeptide processing and other neural functions. *Annu. Rev. Neurosci.* 7:189–222.

29. Lundberg, J. M., and T. Hökfelt. 1983. Coexistence of peptides and classical neurotransmitters. *Trends Neurosci.* 6:325–333.

30. Mahon, A. C., P. E. Lloyd, K. R. Weiss, I. Kupfermann, and R. H. Scheller. 1985. The small cardioactive peptides A and B of *Aplysia* are derived from a common precursor molecule. *Proc. Natl. Acad. Sci. USA.* 82:3925–3929.

31. Mahon, A. C., J. R. Nambu, R. Taussig, M. Shyamala, A. Roach, and R. H. Scheller. 1985. Structure and expression of the egg laying hormone gene family in *Aplysia*. *J. Neurosci.* 5:1872–1880.

32. McAllister, L. B., R. H. Scheller, E. R. Kandel, and R. Axel. 1983. *In situ* hybridization to study the origin and fate of identified neurons. *Science (Wash. DC).* 222:800–808.

33. Nambu, J. R., R. Taussig, A. C. Mahon, and R. H. Scheller. 1983. Gene isolation with cDNA probes from identified *Aplysia* neurons: neuropeptide modulators of cardiovascular physiology. *Cell.* 35:47–56.

34. Price, C. H., and D. J. McAdoo. 1979. Anatomy and ultrastructure of the axons and terminals of neurons R3–14 in *Aplysia*. *J. Comp. Neurol.* 188:647–677.

35. Price, C. H., and D. J. McAdoo. 1981. Localization of axonally transported $^3$H-glycine in vesicles of identified neurons. *Brain Res.* 219:307–315.

36. Price, C. H., W. Fowle, and A. R. Rittenhouse. 1984. Anatomy and innervation of the anterior aorta in *Aplysia* and ultrastructure of specialized neuromuscular junctions on vascular smooth muscle. *J. Comp. Neurol.* 221:186–197.

37. Rayport, S. G., R. T. Ambron, and J. Babiarz. 1983. Identified cholinergic neurons R2 and LP1 control mucus release in *Aplysia*. *J. Neurophysiol.* 49:864–876.

38. Roth, J. 1982. The protein A-gold (p-Ag) technique. Qualitative and quantitative approach for antigen localization on thin sections. *In* Techniques in Immunocytochemistry. G. R. Bullock and P. Petrusz, editors. Academic Press Ltd., London. 107–133.

39. Rothman, B. S., E. Mayeri, R. O. Brown, P-M. Yuan, and J. E. Shively. 1983. Primary structure and neuronal effects of $\alpha$-bag cell peptide, a second candidate neurotransmitter encoded by a single gene in bag cell neurons of *Aplysia*. *Proc. Natl. Acad. Sci. USA.* 80:5753–5757.

40. Rothman, B. S., G. Weir, and F. E. Dudek. 1983. Egg-laying hormone: direct action on the ovotestis of *Aplysia*. *Gen. Comp. Endocrinol.* 52:134–141.

41. Sawada, M., D. J. McAdoo, J. E. Blankenship, and C. H. Price. 1981. Modulation of arterial muscle contraction in *Aplysia* by glycine and neuron R14. *Brain Res.* 207:486–490.

42. Sawada, M., J. E. Blankenship, and D. J. McAdoo. 1981. Neural control of a molluscan blood vessel, anterior aorta of *Aplysia*. *J. Neurophysiol.* 46:967–986.

43. Sawada, M., D. J. McAdoo, M. Ichinose, and C. H. Price. 1984. Influences of glycine and neuron R14 on contraction of the anterior aorta of *Aplysia*. *J. Physiol. Soc. Jpn.* 34:747–767.

44. Schaefer, M., M. Picciotto, T. Kreiner, R. Taussig, and R. H. Scheller. 1985. Identified neurons in *Aplysia* express a gene encoding multiple FMRFamide copies. *Cell.* 41:457–467.

45. Scheller, R. H., J. F. Jackson, L. B. McAllister, J. H. Schwartz, E. R. Kandel, and R. Axel. 1982. A family of genes that codes for ELH, a neuropeptide eliciting a stereotyped pattern of behavior in *Aplysia*. *Cell*. 28:707–719.

46. Scheller, R. H., J. F. Jackson, L. B. McAllister, B. S. Rothman, E. Mayeri, and R. Axel. 1983. A single gene encodes multiple neuropeptides mediating a stereotyped behavior. *Cell*. 35:7–22.

47. Slot, J. W., and H. J. Geuze. 1981. Sizing of protein A-colloidal gold probes for immunoelectron microscopy. *J. Cell Biol.* 90:533–536.

48. Strumwasser, F. 1983. Peptidergic neurons and neuroactive peptides in molluscs: from behavior to genes. *In* Brain Peptides. D. T. Krieger, M. J. Brownstein, and J. B. Martin, editors. John Wiley & Sons Inc., New York. 183–216.

49. Stuart, D. K., A. Y. Chiu, and F. Strumwasser. 1980. Neurosecretion of egg-laying hormone and other peptides from electrically active bag cell neurons of *Aplysia*. *J. Neurophysiol.* 43:488–498.

50. Susswein, A., and M. Benny. 1985. Sexual behavior in *Aplysia fasciata* induced by homogenates of the distal large hermaphroditic duct. *Neurosci. Lett.* 59:325–330.

51. Taussig, R., R-R. Kaldany, and R. H. Scheller. 1984. A cDNA clone encoding neuropeptides isolated from *Aplysia* neuron L11. *Proc. Natl. Acad. Sci. USA*. 81:4988–4992.

52. Taussig, R., R-R. Kaldany, J. B. Rothbard, G. K. Schoolnik, and R. H. Scheller. 1985. Expression of the L11 neuropeptide gene in the *Aplysia* central nervous system. *J. Comp. Neurol.* In press.

53. Wallace, E. F., E. Weber, J. D. Barchas, and C. J. Evans. 1984. A putative processing enzyme from *Aplysia* that cleaves dynorphin A at the single arginine residue. *Biochem. Biophys. Res. Commun.* 199:415–422.

54. Weber, E., C. J. Evans, S. J. Samuelsson, and J. D. Barchas. 1981. Novel peptide neuronal system in rat brain and pituitary. *Science (Wash. DC)*. 214:1248–1251.

55. Weiss, S., J. I. Goldberg, K. S. Chohan, W. K. Stell, G. I. Drummond, and K. Lukowiak. 1984. Evidence for FMRFamide as a neurotransmitter in the gill of *Aplysia californica*. *J. Neurosci.* 4:1994–2000.

56. Wilson, D. L. 1971. Molecular weight distribution of proteins synthesized in single identified neurons of *Aplysia*. *J. Gen. Physiol.* 57:26–40.